Available online at www.sciencedirect.com
ScienceDirect
Ceramics International 37 (2011) 2973–2979
CERAMICS INTERNATIONAL
www.elsevier.com/locate/ceramint

Review paper

Corrosion mechanisms of $Al_2O_3/MgAl_2O_4$ by V_2O_5, NiO, Fe_2O_3 and vanadium slag

B. Fernández *, J.M. Almanza, J.L. Rodríguez, D.A. Cortes, J.C. Escobedo, E.J. Gutiérrez

Centro de Investigación y de Estudios Avanzados del IPN, Carretera Saltillo-Monterrey, Km. 13.5, Ramos Arizpe, Coahuila 25900, Mexico

Received 15 February 2011; received in revised form 18 May 2011; accepted 23 May 2011
Available online 27 May 2011

Abstract

The effects of V_2O_5, NiO, Fe_2O_3 and vanadium slag on the corrosion of Al_2O_3 and $MgAl_2O_4$ have been investigated. The specimens of Al_2O_3 and $MgAl_2O_4$ with the respective oxides above mentioned were heated at 10 °C/min from room temperature up to three different temperatures: 1400, 1450 and 1500 °C. The corrosion mechanisms of each system were followed by XRD and SEM analyses. The results obtained showed that Al_2O_3 was less affected by the studied oxides than $MgAl_2O_4$. Alumina was only attacked by NiO forming $NiAl_2O_4$ spinel, while the $MgAl_2O_4$ spinel was attacked by V_2O_5 forming MgV_2O_6. It was also observed that Fe_2O_3 and Mg, Ni, V and Fe present in the vanadium slag diffused into Al_2O_3. On the other hand, the Fe_2O_3 and Ca, S, Si, Na, Mg, V and Fe diffused into the $MgAl_2O_4$ structure. Finally, the results obtained were compared with those predicted by the FactSage software.

Keywords: C. Diffusion; Corrosion of $Al_2O_3/MgAl_2O_4$; Chemical reaction; Microstructure; FactSage

Contents

1. Introduction

Melting glass furnaces and gasifiers require refractories with good corrosion and erosion resistance. However, the production of refractories with these characteristics has been one of the main problems in the glass melting industry due to the corrosive melting glass and the compounds present in the fuel used inside the furnace. Many refractories have been installed in glass melting furnaces and gasifiers, such as conventional silica (SiO_2), fused cast alumina (Al_2O_3), sintered and fused cast chrome–alumina (Cr_2O_3–Al_2O_3), bonded and fused cast mullite (Al_2O_3–SiO_2), chrome–magnesia spinel (Cr_2O_3–MgO) and bonded fused cast spinel (MgO–Al_2O_3). The Al_2O_3 and $MgAl_2O_4$ were the materials with the highest interest. Godard, Yang, Askel and Liang [1–4] have studied the corrosion of silica, mullite, zirconia, alumina and spinel refractories in melting glass furnaces. They found that, Al_2O_3-based and $MgAl_2O_4$ spinel refractories were the thermodynamically most stable systems. These materials exhibit excellent physical and mechanical properties such as resistance to strong acids and alkalis attack at high temperatures, low thermal expansion and good thermal conductivity, as well as wear resistance, high strength, hardness and stiffness. These

* Corresponding author. Tel.: +52 844 4 38 96 00x9687; fax: +52 844 4 38 96 00x9610.
E-mail address: berenisf@hotmail.com (B. Fernández).

0272-8842/$36.00
doi:10.1016/j.ceramint.2011.05.118

promising properties of both materials Al_2O_3 and $MgAl_2O_4$ spinel offer the potential to be used in different areas such as the cement, copper, steel and glass industries. The production of Al_2O_3 and $MgAl_2O_4$ refractories has attracted attention of a large number of researchers who are trying to produce refractories with the required properties.

On the other hand, there is a worldwide need to economize the industrial processes. For instance, petroleum coke has been used as an alternative to the natural fuel [5]. Also the most of the countries from Latin America have not a strict environmental policy; this allows them the use of pet coke as fuel in different processes. However, it has high vanadium, nickel and iron contents [6], which promote the corrosion and failure of refractories. Therefore, glass producers have focused attention on the study of the interaction between these impurities and the refractories. This had been done before, but the experimentation was only with industrial purposes. Hence the information that is available is scarce and old [7–9]. In fact, the aim of this investigation is to study and compare the corrosion mechanisms of Al_2O_3 and $MgAl_2O_4$ spinel by V_2O_5, NiO, Fe_2O_3 and vanadium slag. Finally, in order to understand the behavior of Al_2O_3 and $MgAl_2O_4$ spinel with these oxides, the FactSage 5.1 thermodynamic software was used to predict the phases (under equilibrium conditions) in complex multi-component systems. The results were compared with those obtained by XRD and SEM.

2. Materials and methods

Calcined alumina (purity of 99.7%), MgO (purity of 81%), Fe_2O_3 (purity of 99%), V_2O_5 (purity of 98%) and NiO (purity of 99%) were the raw materials employed for the present work. It was used alumina with 0.5 wt.% MgO while $MgAl_2O_4$ spinel was obtained by mixing stoichiometric composition. The powders were mixed by milling in a plastic container during 12 h using alumina balls and acetone. The mill-mixed products were then dried in a muffle-type furnace at 100 °C during 8 h. Finally, they were uniaxially pressed at 150 MPa. The resulting specimens were sintered for 4 h at 1600 °C in a high-temperature furnace. The corrosion tests were carried out by covering a disk shaped specimen either Al_2O_3 or spinel (previously moistened with acetone) with V_2O_5, Fe_2O_3, NiO or vanadium slag. Table 1 lists the chemical composition of vanadium slag as determined by X-ray fluorescence (XRF).

The specimens of Al_2O_3 and $MgAl_2O_4$ with the respective oxide were heated at 5 °C/min from room temperature up to three different temperatures: 1400, 1450 and 1500 °C. Holding time was 12 h and the cooling rate was performed at 5 °C/min using air.

The area fraction of porosity and grain size of the Al_2O_3 and $MgAl_2O_4$ samples prior to the corrosion test were determined using an optical microscope and the Image Pro-plus program. Total percentage pore area and mean grain size were obtained from the average of 10 fields (500×) by different color contrast. Meanwhile, the density was determined using a pycnometer due to the small size of the samples. The specimens were milled and the pycnometer was filled with distilled water at 25 °C. Three tests of each sample were done to obtain the result. The approximate bulk density of the specimens was obtained by using the porosity value and the density obtained from the pycnometer.

Microstructural characterization was carried out by scanning electron microscopy (SEM) and X-ray diffraction (XRD) and the alumina/oxide and spinel/oxide interface was analyzed in cross-sections of specimens using back scattered electron (BSE) and chemical microanalyses by EDS.

3. Results and discussion

3.1. Microstructural characterization

The results presented in this investigation correspond to the specimens heat treated at 1500 °C, this is due to the fact that this temperature was the highest used and the results were more representatives. Fig. 1 shows the XRD patterns of Al_2O_3 and $MgAl_2O_4$ registered before and after to the corrosion tests. It has been observed in Fig. 1a, a single phase that corresponds to (α-Al_2O_3) corundum. When Al_2O_3 was exposed to Fe_2O_3 and V_2O_5, there was not a chemical reaction and only the Al_2O_3 phase was detected. However, when Al_2O_3 was exposed to NiO, the $NiAl_2O_4$ spinel was detected indicating the chemical reaction between Al_2O_3 and NiO. The presence of NiO indicates that there was still NiO that has not reacted. In a similar behavior, when Al_2O_3 was exposed to vanadium slag the presence of $MgAl_2O_4$ was detected. The Al_2O_3 sample reacted with the MgO present in the vanadium slag forming the $MgAl_2O_4$ spinel.

Fig. 1b shows the XRD pattern corresponding to the $MgAl_2O_4$ spinel, as it can be seen only this phase was detected. In the case of $MgAl_2O_4$ spinel exposed to Fe_2O_3, the magnesium–iron aluminate spinel was detected as a single phase. This result suggests the diffusion of Fe ions into the $MgAl_2O_4$ spinel structure. After exposing the $MgAl_2O_4$ spinel to V_2O_5, the MgV_2O_6 phase was detected. This indicates that the MgO present in the $MgAl_2O_4$ reacted with the V_2O_5. However, when $MgAl_2O_4$ was exposed to NiO there was a change of $MgAl_2O_4$ to $NiAl_2O_4$. This is due to the similar valence and ionic radius of Mg and Ni, which allows that Ni-ions occupy the Mg interstices into the spinel structure. On the other hand when $MgAl_2O_4$ was exposed to vanadium slag there was no detectable change.

Fig. 2 shows the microstructure of the corundum phase (α-Al_2O_3) and the $MgAl_2O_4$ spinel sintered at 1600 °C. As observed, the alumina phase shows rounded and needle well-defined grains (Fig. 2a). Sintered Al_2O_3 sample contains a grain size distribution from 4 to 15 μm with 7.1 μm as average grain size. The specimen showed intergranular pores from 25 μm to 75 μm in diameter and the porosity of the sample was 16.13%. The bulk density of Al_2O_3 sample was 3.23 g/cm^3.

The $MgAl_2O_4$ spinel exhibits plate-shaped grains (Fig. 2b), the average grain size was 3.4 μm (range 2–13 μm) with a porosity of 5% and pore size ranging from 15 μm to 70 μm. The bulk density of $MgAl_2O_4$ sample was 3.35 g/cm^3. It is well known that the presence of MgO during the processing of Al_2O_3

Table 1
Chemical composition of vanadium slag (wt.%).

Ga_2O_3	0.0158
CoO	0.0171
CuO	0.0239
SrO	0.034
ZnO	0.0392
MoO_3	0.0531
K_2O	0.097
La_2O_3	0.176
P_2O_5	0.196
TiO_2	0.198
MnO	0.35
Cr_2O_3	0.3916
CaO	1.991
Fe_2O_3	2.015
Na_2O	2.7
Al_2O_3	2.19
SiO_2	3.12
MgO	3.513
NiO	5.409
SO_3	8.976
PXC	10.09
V_2O_5	58.39

helps the densification, avoiding abnormal grain growth. Meanwhile, during sintering of $MgAl_2O_4$ spinel at high temperature, the densification and the expansion of material by sintering occur simultaneously.

Fig. 3 shows the cross-section microstructure of Al_2O_3 after being exposed at 1500 °C to Fe_2O_3, V_2O_5, NiO and vanadium slag. Fig. 3a shows the microstructure of Al_2O_3 after being exposed to Fe_2O_3. It can be seen some angular-shaped and dark-gray particles that correspond to Al_2O_3, while the brightest and continuous phase correspond to Fe_2O_3. A third phase was between the Fe_2O_3 and Al_2O_3 particles, which had the composition of Al_2O_3:Fe_2O_3 = 79.27:20.73 as revealed by EDS. The forming phase was an iron aluminate, which had less bright and small rounded-shape particles. It is noteworthy that the Fe_2O_3 and iron aluminate were not detected by XRD. As shown in Fig. 3b, the Fe_2O_3 reacted with alumina and diffused into the Al_2O_3 structure forming an Al_2O_3·Fe_2O_3 compound, which is in agreement with the results of previous studies [10]. Fig. 3c shows the microstructure of Al_2O_3 after being exposed to V_2O_5. In this case, the dark, rounded and needle-shaped particles correspond to Al_2O_3, while the bright and rounded-shaped particles correspond to V_2O_5. The Al_2O_3/V_2O_5 interface was not detected in the sample. Meanwhile the V_2O_5 was found at the top, mid and bottom-thickness of the sample, which indicates penetration of the V_2O_5 into the Al_2O_3. It can be seen in Fig. 3d that when Al_2O_3 is exposed to NiO there was an Al_2O_3/NiO interface, which had a nickel–aluminate spinel composition. The $NiAl_2O_4$ particles were bright with an equiaxial-shape. The dark and needle-shaped crystals correspond to alumina. Fig. 3e shows the effect of the vanadium slag on the microstructure of Al_2O_3. As can be observed, the morphology was a dense and continuous layer at the top and below of the sample, the flake-like particles correspond to Al_2O_3. It was observed that this dense and bright phase at the top contains mainly Al_2O_3 and also had small amounts of impurities presented in the slag (Al_2O_3:NiO:MgO:-Fe_2O_3:V_2O_5 = 60.89:29.11:6.90:1.76:1.34). The Ni, Mg, Fe and V ions diffused into the Al_2O_3 structure. The NiO and MgO reacted with alumina forming spinels. These observations were confirmed by EDS analysis as observed in Fig. 3f.

Fig. 4 shows the microstructure of the $MgAl_2O_4$ spinel attacked with Fe_2O_3, V_2O_5, NiO, and vanadium slag. The $MgAl_2O_4$/Fe_2O_3 interface in Fig. 4a shows three types of bright phases present in the microstructure. These phases correspond to $Mg(Fe,Al)_2O_4$ spinels [11]. The Fe-ions diffused into the spinel structure substituting the Al-ions, this phenomenon has beed reported previously [12]. Therefore the brightest phase has more Fe_2O_3. The Fe_2O_3 as a single phase was not found. Fig. 4c shows the microstructure of $MgAl_2O_4$ spinel corroded by V_2O_5. As it can be seen, there are three types of phases present in the microstructure, the bright, small and rounded-shaped crystals correspond to MgV_2O_6, the dark gray and angular-shaped particles corresponds to $MgAl_2O_4$, and the gray and needle-shaped phase corresponds to some particles of Al_2O_3. MgV_2O_6 was formed by the reaction between the MgO present in the spinel and the V_2O_5. This compound has a low melting point and it is considered detrimental to the mechanical properties. When the $MgAl_2O_4$ spinel was exposed to NiO, the presence of $MgAl_2O_4$, Al_2O_3, NiO and $NiAl_2O_4$ was observed (Fig. 4d). As observed, the morphology of these phases is quite different. The gray particles that correspond to Al_2O_3 and $MgAl_2O_4$ exhibit angular and rounded shape, respectively. However, the bright particles corresponding to the $NiAl_2O_4$ and NiO have regular and irregular spherical particles. Thus, it can be concluded that the $NiAl_2O_4$ results from the diffusion of Ni into the $MgAl_2O_4$

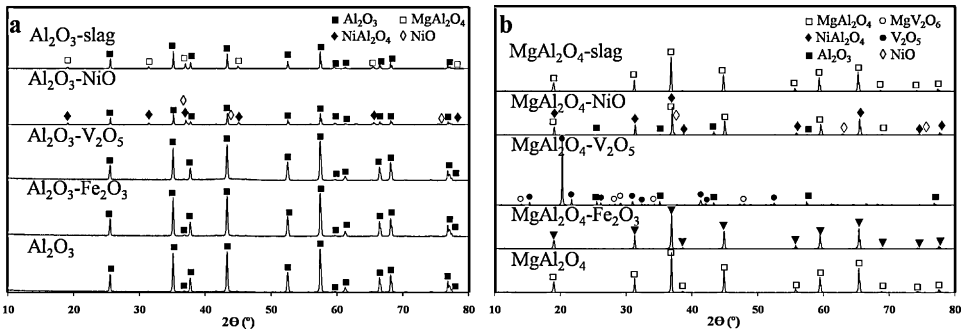

Fig. 1. XRD patterns of (a) Al_2O_3 and (b) $MgAl_2O_4$ registered: before and after being attacked with Fe_2O_3, V_2O_5, NiO and vanadium slag.

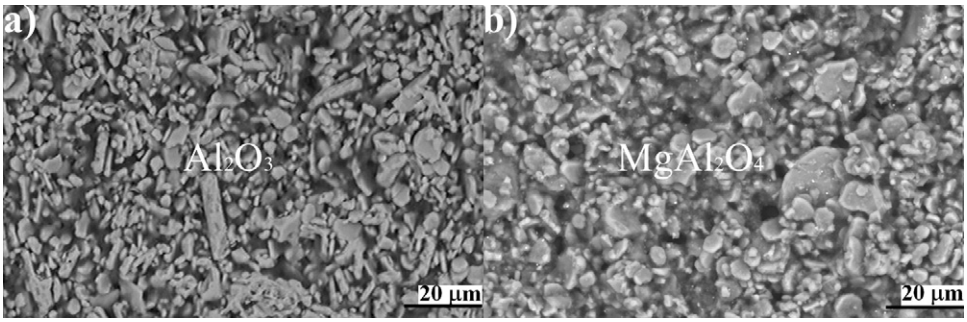

Fig. 2. Cross section microstructures of (a) Al_2O_3 and (b) $MgAl_2O_4$ before corrosion test.

spinel structure [13]. Therefore, the $MgAl_2O_4$ spinel was replaced by the $NiAl_2O_4$ spinel, which is considered a ceramic with a high melting point. However, the structural changes occured from $MgAl_2O_4$ to $NiAl_2O_4$ spinel may affect the mechanical properties. The microstructure of the $MgAl_2O_4$ attacked with the vanadium slag is shown in Fig. 4e. The morphology of the sample consists of agglomerates of two phases. In a similar way than in specimens attacked with V_2O_5, the MgV_2O_6 is observed, but in this case it has Al_2O_3 into its structure.

It can be observed that at a certain distance from surface, there were found some particles containing elements from the slag, such as Na, Mg, Si, S, Ca, V and Fe. This indicates the diffusion of ions to the center of the sample which can form stable phases as spinels, vanadates and silicates. The processing conditions used in this work make it difficult to determine the formation of these phases. However, this information can be explained better by the thermodynamic predictions which are shown in the following section.

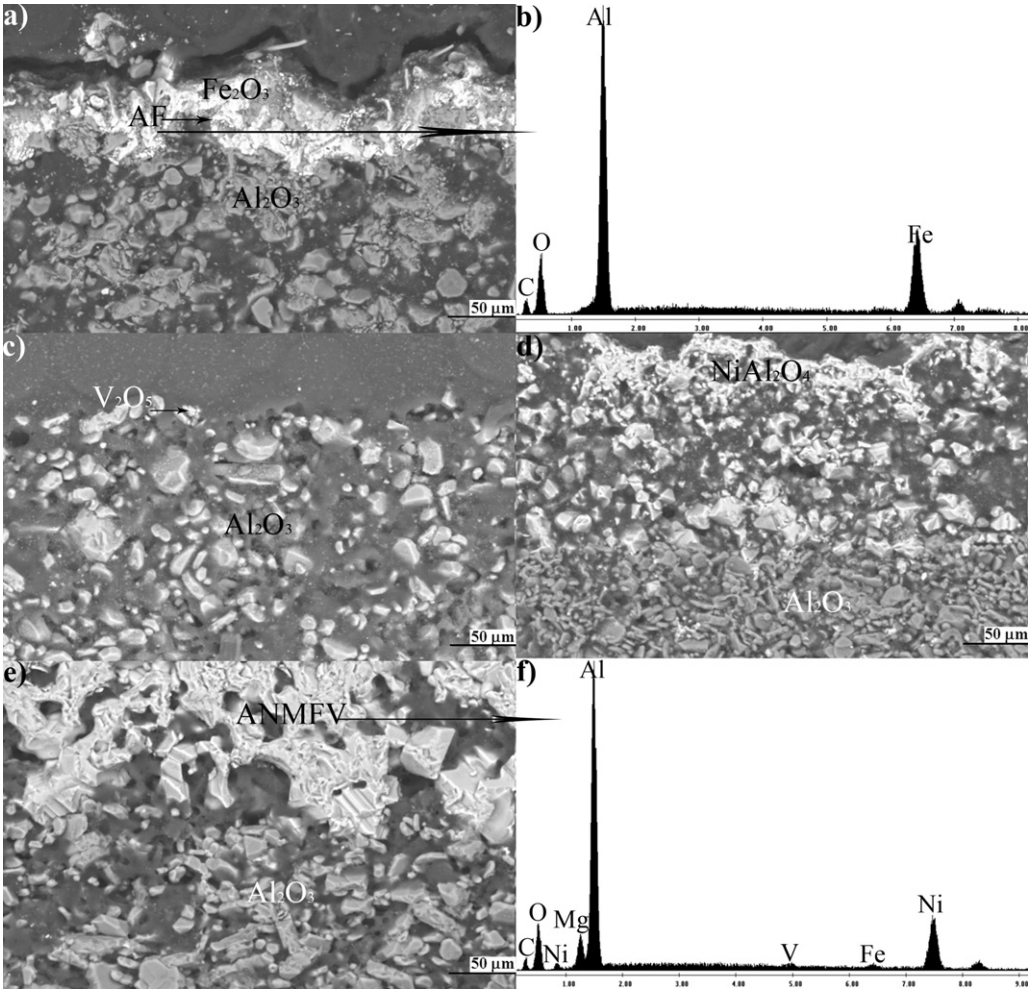

Fig. 3. Cross section microstructures of Al_2O_3 after the attack with (a) Fe_2O_3, (b) EDS analysis, (c) V_2O_5, (d) NiO, (e) vanadium slag and (f) EDS analysis.

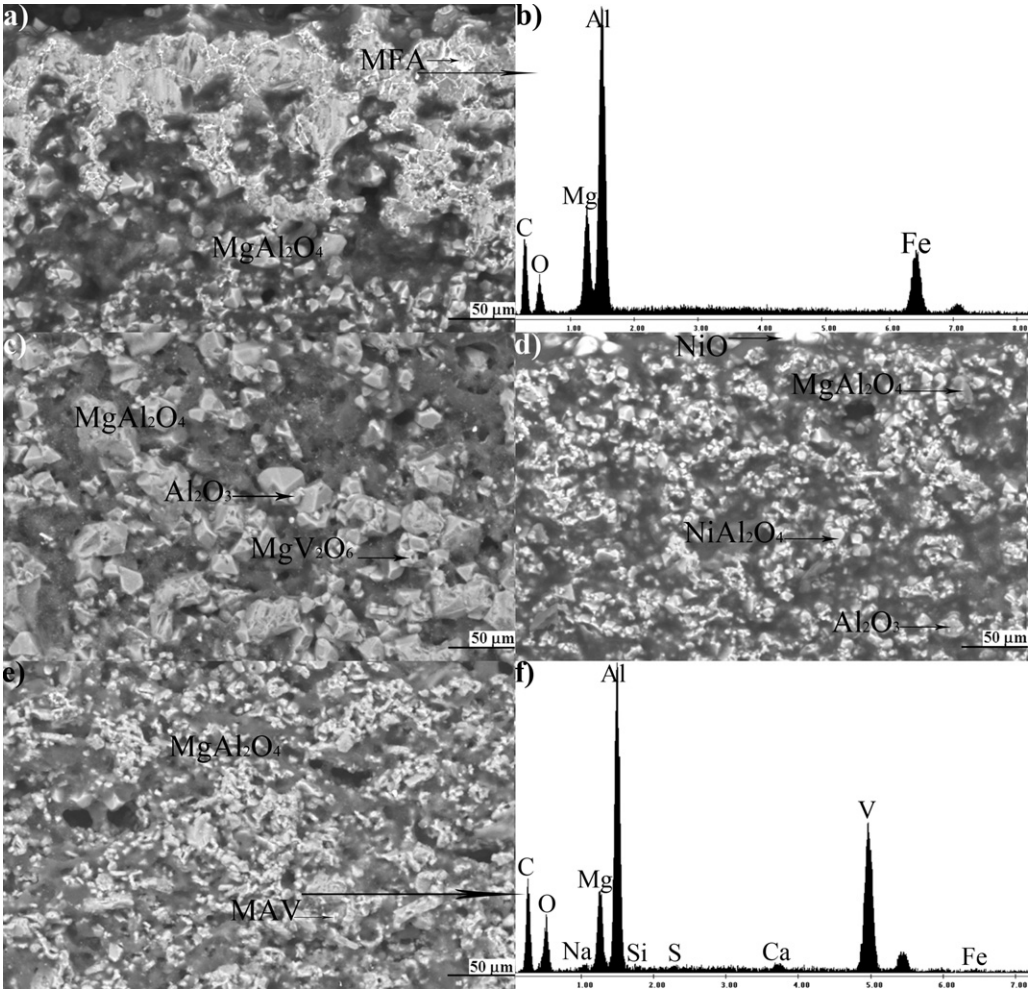

Fig. 4. Cross section microstructures of $MgAl_2O_4$ after being attacked with (a) Fe_2O_3, (b) EDS analysis, (c) V_2O_5, (d) NiO, (e) vanadium slag and (f) EDS analysis.

3.2. FactSage predictions

The prediction of the phases resulting from the attack of Al_2O_3 and $MgAl_2O_4$ by Fe_2O_3, V_2O_5, NiO and vanadium slag, was obtained by the FactSage 5.1 software, which allows to predict the compounds that can be formed during corrosion under equilibrium conditions [14,15].

Table 2 shows the predicted phases of Al_2O_3 system corroded with the different oxides. As it can be seen, in the Al_2O_3–Fe_2O_3 system, the $Fe_2Al_2O_6$ phase is formed at the three studied temperatures (Table 2) according to the Al_2O_3–Fe_2O_3 equilibrium phase diagram [16]. The $Fe_2Al_2O_6$ formation predicted by the program was consistent with the result obtained in this work. However, the $Fe_2Al_2O_6$ was found only on the reaction interface between the two materials. The alumina sample was not completely converted to $Fe_2Al_2O_6$, due to the fact that the exposure time was not enough to reach equilibrium (1 mol of Al_2O_3 and 1 mol of Fe_2O_3). For the Al_2O_3–V_2O_5 system at 1400 °C the thermodynamic analysis did not predicted any change. But at higher temperatures, there was a reduction from V_2O_5 to VO_2. The VO_2 was not present in the results obtained. This is due to that VO_2 is stable only at high temperature and the most stable phase at room temperature is V_2O_5. During the heating the V_2O_5 is reduced and transforms to VO_2 [17]. But at the cooling stage the VO_2 was oxidized again to V_2O_5. It was predicted by FactSage software that the

Table 2
Phases predicted by FactSage for Al_2O_3 at 1400, 1450 and 1500 °C.

	1400 °C	1450 °C	1500 °C
Al_2O_3–Fe_2O_3	$Fe_2Al_2O_6$	$Fe_2Al_2O_6$	$Fe_2Al_2O_6$
Al_2O_3–V_2O_5	Al_2O_3, V_2O_5	Al_2O_3, VO_2	Al_2O_3, VO_2
Al_2O_3–NiO	$NiAl_2O_4$	$NiAl_2O_4$	$NiAl_2O_4$
Al_2O_3–vanadium slag	Al_2O_3, VO_2, $MgAl_2O_4$, $NiAl_2O_4$, $NaAlSiO_4$, $Ca_2V_2O_7$, $Na_2V_2O_6$, $Fe_2Al_2O_6$	Al_2O_3, VO_2, $MgAl_2O_4$, $NiAl_2O_4$, $NaAlSiO_4$, $Ca_2V_2O_7$, $Na_2V_2O_6$, $Fe_2Al_2O_6$	Al_2O_3, VO_2, $MgAl_2O_4$, $NiAl_2O_4$, $NaAlSiO_4$, $CaAl_{12}O_{19}$, $Na_2V_2O_6$, $Fe_2Al_2O_6$

Table 3
Phases predicted by FactSage for $MgAl_2O_4$ spinel at 1400, 1450 and 1500 °C.

	1400 °C	1450 °C	1500 °C
$MgAl_2O_4$–Fe_2O_3	$MgAl_2O_4$, Fe_2O_3	$MgAl_2O_4$, Fe_3O_4, $Fe_2Al_2O_6$	$MgAl_2O_4$, Fe_3O_4, $Fe_2Al_2O_6$
$MgAl_2O_4$–V_2O_5	$MgAl_2O_4$, V_2O_5	$MgAl_2O_4$, VO_2, Al_2O_3	$MgAl_2O_4$, VO_2, Al_2O_3
$MgAl_2O_4$–MgV_2O_6	$MgAl_2O_4$, V_2O_5, $Mg_2V_2O_7$	$MgAl_2O_4$, VO_2, $Mg_2V_2O_7$	$MgAl_2O_4$, VO_2, $Mg_2V_2O_7$
	500 °C	700 °C	
$MgAl_2O_4$–V_2O_5		Al_2O_3, MgV_2O_6	
$Mg_2V_2O_7$–VO_2–O_2	MgV_2O_6, $Mg_2V_2O_7$		
$MgAl_2O_4$–NiO	$MgAl_2O_4$, NiO	$MgAl_2O_4$, NiO	$MgAl_2O_4$, NiO
$MgAl_2O_4$–vanadium slag	$MgAl_2O_4$, VO_2, NiO, $Mg_2V_2O_7$, $Na_2V_2O_7$, $Ca_2V_2O_7$, $NiFe_2O_4$, $Na_2Al_2Si_6O_{16}$	$MgAl_2O_4$, VO_2, NiO, Mg_2SiO_4, $Na_2V_2O_7$, $Ca_2V_2O_7$, $NiFe_2O_4$, $Na_2Al_2Si_6O_{16}$	$MgAl_2O_4$, VO_2, NiO, Mg_2SiO_4, $Na_2V_2O_7$, $Ca_2V_2O_7$, $NaAlSiO_4$, $NiFe_2O_4$

Al_2O_3 reacted with NiO forming the $NiAl_2O_4$ spinel. However, the results of XRD and SEM demonstrated that the $NiAl_2O_4$ spinel co-exists with NiO and Al_2O_3. This observation may be associated to the fact that equilibrium was not reached. In the Al_2O_3-vanadium slag system, the same phases were found as predicted for temperatures of 1400 and 1450 °C. While, at 1500 °C, only the replacement of $Ca_2V_2O_7$ by $CaAl_{12}O_{19}$ is observed. The $Fe_2Al_2O_6$, Al_2O_3, VO_2 and $NiAl_2O_4$ phases are in agreement with the phases predicted by the thermodynamic analysis in the Al_2O_3–Fe_2O_3, Al_2O_3–V_2O_5 and Al_2O_3–NiO systems, respectively. However the presence of all these phases is below of the amount for the detection limit by XRD, therefore their identification was limited to that observed by EDS.

Table 3 shows the phases predicted for the corrosion of $MgAl_2O_4$ by the different oxides. For the $MgAl_2O_4$–Fe_2O_3 system was not observed any change at 1400° C, but at 1450 °C some changes start to occur and the same behavior is observed at 1500 °C. This changes are in agreement with a previous work [12], which states that the Fe_2O_3 and Al_2O_3 reacts to form an spinel structure at high temperatures. The thermodynamic analysis for the $MgAl_2O_4$–V_2O_5 and Al_2O_3–V_2O_5 systems, predicted the presence of VO_2, which oxidize during the cooling stage. While the MgV_2O_6 was not predicted by the thermodynamic analysis, it was necessary to figure out the presence of this phase through the study using lower temperatures as can be seen in Table 3. The thermodynamic analysis confirmed the MgV_2O_6 and $Mg_2V_2O_7$ formation at lower temperatures. Therefore during the cooling stage, these phases were present as liquid in the sample. In the case of $MgAl_2O_4$ being attacked with NiO, it was not predicted any interaction independently of the temperature (from 1400 to 1500 °C). Finally, in the $MgAl_2O_4$-vanadium slag system, there was many phases formed by reaction of $MgAl_2O_4$ with the elements present in the slag (Table 3). Although these phases were not detected by XRD, they were detected by EDS analysis.

In the systems Al_2O_3-oxides and $MgAl_2O_4$-oxides, the XRD and SEM-EDS analysis did not identify some phases which were predicted by the thermodynamic analysis, due to the small amounts of these phases which are below of the detection limits of these techniques and the exposure time was not enough for them to be formed. As well it is important to mention that the formation of most of these phases can affect the stability of the refractory material. This is due to that these phases diffuse into a porous structure and then the phases condense on the pores affecting the properties of the refractory material.

4. Conclusions

The results of the present investigation show the corrosion mechanisms of Al_2O_3 and $MgAl_2O_4$ spinel by Fe_2O_3, V_2O_5, NiO or vanadium slag. These mechanisms can be summarized as follows:

(a) In the Al_2O_3–Fe_2O_3 and Al_2O_3–V_2O_5, there was no chemical reaction between the phases. In contrast, for the Al_2O_3–NiO system, there was a chemical reaction resulting in the formation of $NiAl_2O_4$. Finally, in the Al_2O_3-vanadium slag system, there was a diffusion of the elements present in the slag into the Al_2O_3 structure.
(b) In the $MgAl_2O_4$–Fe_2O_3 system there was a diffusion of iron into the spinel structure, while in the $MgAl_2O_4$–vanadium slag system, the elements present in the slag such as Ca, S, Si, Na and V diffused into the $MgAl_2O_4$. However, it was not observed a chemical reaction in these two systems. In the case of the $MgAl_2O_4$–V_2O_5, a chemical reaction between these phases occurred resulting in the formation of MgV_2O_6. Finally, for the $MgAl_2O_4$–NiO system, there was a replacement of Ni ions by the Mg ions resulting in the formation of a $NiAl_2O_4$ spinel.
(c) From these results it can be concluded that the Al_2O_3 is less affected by the studied oxides than $MgAl_2O_4$.

Acknowledgments

The authors of this work would like to thank CONACyT, Martha Rivas and Sergio Rodríguez for their valuable time and contributions through this study.

References

[1] H.T. Godard, L.H. Kotacska, J.F. Wosinki, S.M. Winder, A. Gupta, K.R. Selkregg, S. Gould, Refractory corrosion behavior under air–fuel and oxy–fuel environments, in: C.H. Drummond (Ed.), A Collection of Papers

Presented at the 57th Conference on Glass Problems: Ceramics Engineering and Science Proceedings, vol. 18, John Wiley and Sons Inc., New Jersey, 1997, pp. 260–262.
[2] H.Y. Yang, C.F. Chan, Corrosion resistance and microstructure of high-alumina refractories, based on the rotary slag test, J. Am. Ceram. Soc. 73 (1990) 1074–1077.
[3] C. Askel, The microstructural features of an alumina–mullite–zirconia refractory material corroded by molten glass, Ceram. Int. 29 (2003) 305–309.
[4] H. Sarpoolaky, S. Zhang, W.W. Lee, Corrosion of high alumina and near stoichiometric spinels in iron-containing silicates slags, J. Eur. Ceram. Soc. 23 (2003) 293–300.
[5] J. Chen, X. Lu, Progress of petroleum coke combusting in circulating fluidized bed boilers—a review and future perspectives, Resour. Conserv. Recycl. 49 (2007) 203–216.
[6] X. Zhang, J. Jia, Z. Zhou, F. Wang, Influence of blending methods on the co-gasification reactivity of petroleum coke and lignite, Energy Convers. Manage. 52 (2011) 1810–1814.
[7] G. Christof, O. Mauschitz, Glass tank regenerators—modern refractory lining materials and attack from V_2O_5, Glass 61 (1984) 99–102.
[8] G.S. Dhupia, E. Guerenz, W. Kranert, M. Metzeger, Test of refractory materials for the condensation zone of regenerators, Mater. Sci. Forum 34 (1998) 767–774.
[9] R.W. Brown, K.H. Sandmeyer, Sodium vanadate effect over refractory superstructures, Glass Ind. Mag. 59 (1978) 16.
[10] A. Maun, C.L. Gee, J. Am. Ceram. Soc. 39 (1956) 207–214.
[11] Y.K. Paek, B.K. Lee, S.L. Kang, Discontinuous dissolution of iron aluminate spinel in the Al_2O_3–Fe_2O_3 system, J. Am. Ceram. Soc. 78 (1995) 2149–2152.
[12] M.K. Cho, G.G. Hong, S.K. Lee, Corrosion of spinel clinker by CaO–Al_2O_3–SiO_2 ladle slag, J. Eur. Ceram. Soc. 22 (2002) 1783–1790.
[13] M. Serra, P. Salagre, Y. Cesteros, F. Medina, J. Sueiros, Design of NiO–MgO materials with different properties, Phys. Chem. Chem. Phys. 6 (2004) 858–864.
[14] FactSage™, Fact XML 5.2. CRCT and GTT-Technologies, Fact Sage Thermochemical Software and Database, Canada and Germany (2002).
[15] L.I. Hanxu, Y. Ninomiya, D. Zhongbing, Z. Minyxu, Application of the FactSage to predict the ash melting behavior in reducing conditions, Chin. J. Chem. Eng. 14 (2006) 784–789.
[16] A. Muan, Am. J. Sci. 420 (1958).
[17] Y. Ninguyi, L. Jinhua, L. Chenglu, Valance reduction process from sol–gel V_2O_5 to VO_2 thin films, Appl. Surf. Sci. 191 (2002) 176–180.